Characteristic Parameters Estimation of Uncertainties Present in an Active Magnetic Bearing Integrated Flexible Rotor System Using Dynamic Reduction Technique

Sampath Kumar Kuppa and Mohit Lal(✉)

Department of Industrial Design, National Institute of Technology Rourkela, Rourkela 769008, Odisha, India
{515idl003, lalm}@nitrkl.ac.in

Abstract. In this article, an identification algorithm is developed to estimate the characteristic parameters of uncertainties present in rotating machines. A dynamic system consists of two flexible shafts each having a rigid disc and an active magnetic bearing (AMB) at its mid–span, mounted on flexible bearings at ends and connected together with a flexible coupling is considered for numerical simulation. Finite element method (FEM) is used to obtain dynamic equations of motion (EOMs) for coupled flexible rotor system integrated with AMBs. An identification algorithm based on least squares technique is developed to estimate the characteristic parameters of uncertainties/faults (i.e., bearing, coupling and residual unbalance) present in the rotor system. FEM is more accurate and realistic approach to model real rotor test rigs but degrees of freedom (DOFs) of the system increases as the number of nodes increases. Accessibility of these DOFs and accurate displacement measurements are the most challenging problems in the real rotor test rigs. To overcome this difficulty, a dynamic reduction technique is applied in the developed identification algorithm to eliminate some linear and all angular DOFs (that are practically immeasurable and to avoid difficulties of number of sensors). A Proportional Integral Derivative (PID) controller is used to obtain the controlling current for AMBs to stabilize the rotor system. The EOMs derived is solved by fourth order Runge–Kutta method to generate the displacement and current responses. The time domain responses are converted into frequency domain using Fast Fourier Transform (FFT). Full spectrum analysis is performed to estimate the desired characteristic parameters. The effectiveness of the algorithm is checked for measurement error and found to be excellent.

Keywords: Active magnetic bearing · Dynamic reduction · Full spectrum FFT analysis · PID controller

1 Introduction

Vibration minimization is an important task to practitioner for safe and efficient functioning of all rotating machines. The most common faults associated with rotating machinery are misalignment and inherent unbalance that causes severe vibration and

K. L. Cavalca and H. I. Weber (Eds.): IFToMM 2018, MMS 63, pp. 234–248, 2019.
https://doi.org/10.1007/978-3-319-99272-3_17

leads to catastrophic failure of the system, high economic loss to industries, sometimes even worse loss of human lives etc. Characteristic parameters associated with these faults need to be detected at early stage for smooth functioning of the rotating machinery. In recent trend, Active Magnetic bearings (AMB) are tremendously used in high–speed rotating machines to actively control the dynamic system under the influence of different faults or uncertainties present in the rotor system.

[1] presented a new effective method of dynamic condensation, which reduces the order of dynamic matrices without introducing further approximation by representing the passive co-ordinates in terms of the active ones exactly. The resulting frequency dependent eigenvalue problem is solved by a combined technique of Sturm sequence and subspace iteration. [2] proposed a modification to the dynamic condensation; this decreases the number of numerical operations useful for application of the method and reduces the computational time. [3] developed an algorithm to identify the faults in rotor–AMB system in frequency domain, and designed a controller based on Linear–Quadratic (LQ) controller to improve the performance of the rigid rotor system with Multi–Input Multi–output (MIMO) AMB. [4] concluded that condition monitoring techniques play a major role in the rotating machinery, to detect and classify different faults in the machineries. It has been used for many years with improvements in the algorithms to estimate various faults in the machines such as cracks, unbalance, bends and misalignment. [5] proposed a technique to control active vibration of the rotor shaft using the electromagnetic exciter with the PD (proportional derivative) controller. The exciter reduces the vibration due to the non–contact control force and increase the stability of the rotor even at high speeds with safer operations. Many researchers [7–10, 12] estimated bearing and coupling parameters numerically and experimentally, without AMB. [11] proposed an identification technique based on the frequency response to estimate the unknown parameters of the flexible rotor system with AMB. The technique is validated on three different AMB models. [13] developed a model based switching crack identification algorithm with the help of dynamic condensation scheme to estimate the crack stiffness, viscous damping, unbalance and AMB parameters of a Jeffcott rotor. [14] proposed a methodology based on rotor unbalance response to identify the closed loop AMB stiffness and damping parameters of a flexible rotor system with AMB. In finite element method (FEM) modelling is done to obtain equations of motion and errors are estimated for each parameter. The proposed method is validated with the experiments, and observed that the numerical results are very close to experimental results. [15] developed an identification algorithm to estimate the stiffness and damping of the flexible rotor AMB system in the presence of unknown residual unbalance. They concluded unknown residual unbalances reduce the identification accuracy and a rigid rotor model is only valid when the rotating speed is far below the first critical speed.

An identification algorithm based on least squares technique is developed to estimate the characteristic parameters of uncertainties/faults present in the rotor system. Although, finite element method (FEM) is adopted as more accurate and realistic approach to model real rotor test rigs, however, the main problem is degrees of freedom (DOFs) of the system that increases as the number of nodes increases. Accessibility of all DOFs and measurement of angular DOFs are the most challenging problems in the real rotor test rigs. To overcome this difficulty, a dynamic reduction technique is

applied in the developed identification algorithm to eliminate some linear and all angular DOFs (that are practically immeasurable and to avoid difficulties of number of sensors). Numerical model consists of two flexible shafts each have a rigid disc and an AMB at its mid–span, mounted on flexible bearings at the ends and connected together with a flexible coupling is considered. For FE formulation, the shaft is modelled using Euler Bernoulli beam theory. A proportional integral derivative (PID) controller is used to obtain the controlling current for AMBs to stabilize the rotor system. The equation of motions (EOM) derived is solved by fourth order Runge–Kutta method to generate the displacement and current responses using SIMULINK^{TM}. The time domain responses are converted into frequency domain using Fast Fourier Transform (FFT). Full spectrum analysis is performed to estimate the desired characteristic parameters. The effectiveness of the algorithm is checked for measurement error and modelling error and found to be excellent.

2 Modelling of the System

Present section deals with the assumptions involved in the modeling of the flexible rotor–bearing–coupling along with AMB. An AMB integrated flexible rotor–bearing–coupling system as shown in Fig. 1, is considered to develop the identification methodology. Euler Bernoulli beam theory is used to model the flexible shaft and the dynamic EOMs of the system are derived by using FEM. Each shaft is mounted on two identical bearings at ends. Bearings are modeled as having linearized distinct stiffness $\left(k_{ij}^{B_n}\right)$ parameters (all bearings have distinct the direct as well as coupled coefficients i.e. $i, j = x, y$ and $n = 1, 2, 3, 4$; for four bearings). Similarly coupling is modeled as having linearized direct, cross–coupled as well as angular stiffness $\left(k_{xx}^{C}, k_{xy}^{C}, k_{yx}^{C}, k_{yy}^{C}, k_{\varphi x}^{C} \,\&\, k_{\varphi y}^{C}\right)$ parameters. Apart from conventional direct and cross–coupled stiffness parameters, additional angular stiffness is considered. Coupling defects are accommodated in the model in terms of misalignment forces and moments [7]. Superscripts '*B*' and '*C*' represent bearing and coupling, respectively.

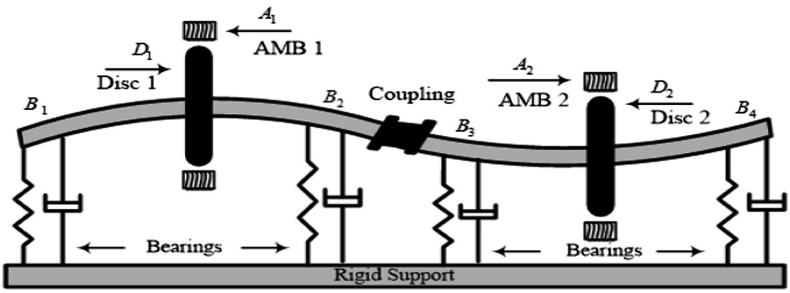

Fig. 1. AMB integrated flexible rotor system

2.1 Shaft Model

The shaft is divided into finite number of elements as shown in Fig. 2. The EOM for 'i^{th}' shaft element could be expressed as,

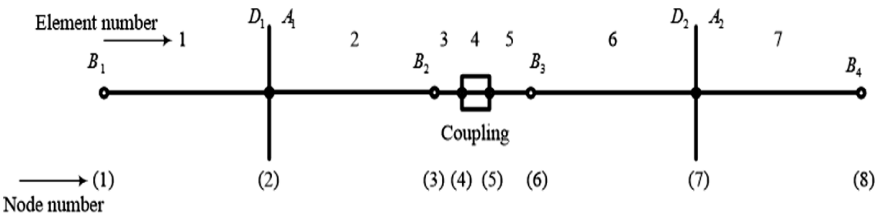

Fig. 2. FE model of the AMB integrated flexible rotor system

$$\bar{M}^S\ddot{v}^S + \left(\bar{C}^S - \omega\bar{G}^S\right)\dot{v}^S + \bar{K}^S v = \bar{f}^S \tag{1}$$

With

$$v = \left\{ u_{x_i} \quad \varphi_{y_i} \quad u_{y_i} \quad \varphi_{x_i} \quad u_{x_{i+1}} \quad \varphi_{y_{i+1}} \quad u_{y_{i+1}} \quad \varphi_{x_{i+1}} \right\}'$$

where superscript 'S' represents shaft. v^S and $\bar{f}^S$ are the elemental nodal displacement and force vectors respectively.$\bar{C}^S$, $\bar{G}^S$, $\bar{K}^S$ and $\bar{M}^S$ are elemental damping, gyroscopic, stiffness and mass matrices of the shaft and details are given in [6].

2.2 Rigid Disc Model

Rigid discs are modeled as having the mass and mass moment of inertia terms at its nodal position. The EOM for disc element could be expressed as,

$$\bar{M}^D\ddot{v}^D - \omega\bar{G}^D\dot{v}^D = \bar{f}^D \tag{2}$$

where superscript 'D' represents disc. v^D and $\bar{f}^D$ are the disc nodal displacement and force vectors respectively. $\bar{M}^D$ and $\bar{G}^D$ are the disc mass and gyroscopic matrices respectively; details are given in [6].

2.3 Bearing Model

The EOM for bearing element could be expressed as,

$$\bar{K}^B v^B = \bar{f}^B \tag{3}$$

where superscript 'B' represents bearing. v^B and $\bar{f}^B$ are the bearing nodal displacement and force vectors, respectively. $\bar{K}^B$ is the bearing stiffness matrix and details are given in [9].

2.4 Residual Unbalance Force Model

The inherent unbalance force vector is defined as

$$\bar{f}_{unb} = me_n\omega^2 e^{j(\omega t+\beta_n)} \tag{4}$$

where $\bar{f}_{unb}$ is the residual unbalance force vector for each disc. The force due to the residual unbalance is defined in terms of magnitude (me_n) and orientation (β_n) of the unbalance, where n = 1, 2; number of discs.

2.5 Coupling Model

The effect of misalignment forces and moments of the coupling is considered in the form of restoring forces (in terms of stiffness). The EOM for coupling element could be expressed as [9],

$$\bar{K}^C v^C = \bar{f}^C \tag{5}$$

Where v^C is the coupling nodal displacement (u_x & u_y and φ_x & φ_y are the linear and angular displacement in two orthogonal directions). Details of $\bar{K}^C$ and v^C are given in [9].

2.6 AMB Model

The magnetic force exerted on the rotor by the AMB can be attributed to two factors, the coil current and the air gap. Thus, the magnetic force exerted on the rotor is given as,

$$\bar{f}_{AMB} = \begin{Bmatrix} -k_{s_x}u_x + k_{i_x}i_x \\ -k_{s_y}u_y + k_{i_y}i_y \end{Bmatrix} \tag{6}$$

A feedback control loop is used to determine the i_x and i_y based on the instantaneous value of u_x and u_y. Here k_s and k_i are the displacement and current stiffness along x and y directions, respectively. In the present work a PID controller is used for tuning and stabilization of the system. The expression for the current output of a PID controller in coils for the force in a particular direction is given as,

$$i_c = k_p u + k_D \dot{u} + k_I \int u \tag{7}$$

where k_p, k_D and k_I are the proportional, differential and current gain. And u is the displacement of the controlling current with respect to time.

2.7 Assembled EOM of the Rotor Bearing Coupling System with AMB

EOM for the complete rotor system could be obtained by combining Eqs. (1)–(6), i.e., the elemental EOMs obtained for the shaft, disc, bearing, coupling, unbalance and AMB force, respectively as,

$$\bar{M}^G\ddot{v} + \left(\bar{C}^G - \omega\bar{G}^G\right)\dot{v} + \bar{K}^G v = \bar{f}_{unb} - \bar{f}_{AMB} \tag{8}$$

with

$$\bar{M}^G = \bar{M}^S + \bar{M}^D; \bar{C}^G = \bar{C}^S; \bar{G}^G = \bar{G}^S + \bar{G}^D; \bar{K}^G = \bar{K}^S + \bar{K}^B + \bar{K}^C;$$

where superscripts B, C, D, G and S represent bearing, coupling, disc, global and shaft respectively. $\bar{M}^G, \bar{C}^G, \bar{G}^G$ & $\bar{K}^G$ represent the global mass, damping, gyroscopic and stiffness matrices, respectively.

2.8 Simulated Responses for Estimation

The AMB and rotor–bearing–coupling parameters used for simulation is listed in Table 1. To generate simulated displacement and current response, Eq. (8) is imported into SIMULINK™ model developed. The time domain equation is solved by fourth–order Runge–Kutta method, to generate the displacement and current responses at different operating speeds. The displacement and the current response obtained in time domain from SIMULINK™ is converted into frequency domain by using the Fast Fourier Transform (FFT) technique. For brevity and completeness, a typical variation of displacement and current response with respect to time at operating frequency (F_r = 19 Hz) in two orthogonal directions i.e., horizontal and vertical direction and orbit plots are shown in Fig. 3. With the help of FFT, the time domain responses (displacement and current) are converted into frequency domain. A typical full spectrum plot obtained for displacement and current responses at 'F_r = 19 Hz' is shown in Fig. 4. From Fig. 4, it could be observed that a peak for operating frequency (F_r) is appearing at F_r + 1, apart from this some other peaks on positive side at (1 Hz, 50 Hz, 124 Hz and 149 Hz) and negative side ($-F_r$ Hz, −49 Hz, −123 Hz and −148 Hz) is appreciable. The positive side peaks are shifted by +1 Hz due to axis arrangement to plot full spectrum. The peak at 1 Hz is due to the static deflection (mass of the rotor system) whereas other peaks on both positive and negative is due to the characteristic phenomena such as system damping, resonance, phase shift, leakage error and signal sampling rate. To analyze the effectiveness of the algorithm against different modes of excitation displacement and current responses are generated at selected operating speeds, in between 2nd and 3rd natural frequency. The first eight natural frequencies of the system are (f_{nf1} = 10.52 Hz, f_{nf2} = 10.68 Hz, f_{nf3} = 31.84 Hz, f_{nf4} = 33.17 Hz, f_{nf5} = 55.33 Hz, f_{nf6} = 57.95 Hz, f_{nf7} = 82.38 Hz, and f_{nf8} = 85.50 Hz).

Table 1. Specifications of the AMB integrated flexible rotor system

Parameters	Values (units)	Parameters	Values (units)
Rotor			
Disc mass m_1 & m_2	2 kg	Shaft length l	2.5 m
Diametrical moment of inertia I_{d1} & I_{d2}	2.4×10^{-3} kg-m^2	Disc eccentricity e_1 & e_2	2.4 μm
Shaft diameter d	0.016 m	Shaft density ρ	7850 kg-m^3
Rayleigh's coefficient for the damping proportional	$a_0 = 1.28$ $a_1 = 7.87 \times 10^{-6}$	Phase change $\beta 1$ & $\beta 2$	30° and 36°
AMB			
Current stiffness, k_{ix1} & k_{ix2}	42.1 N/A	PID	
Displacement stiffness, k_{sx1} & k_{sx2}	1.05×10^5 N/m	Proportional K_p	8400 A/m
Current stiffness, k_{iy1} & k_{iy2}	42.1 N/A	Derivative K_d	13 –s-m^{-1}
Displacement stiffness, k_{sy1} & k_{sy2}	1.05×10^5 N/m	Integral K_I	12800 A/(m-s)

Bearing (stiffness parameters (N/m))							
$K_{xx}^{B_1}$	2.50×10^5	$K_{xy}^{B_1}$	1.20×10^3	$K_{yx}^{B_1}$	1.35×10^3	$K_{yy}^{B_1}$	2.75×10^5
$K_{xx}^{B_2}$	2.75×10^5	$K_{xy}^{B_2}$	1.46×10^3	$K_{yx}^{B_2}$	1.39×10^3	$K_{yy}^{B_2}$	2.82×10^5
$K_{xx}^{B_3}$	2.27×10^5	$K_{xy}^{B_3}$	1.31×10^3	$K_{yx}^{B_3}$	1.44×10^3	$K_{yy}^{B_3}$	2.53×10^5
$K_{xx}^{B_4}$	2.14×10^5	$K_{xy}^{B_4}$	1.21×10^3	$K_{yx}^{B_4}$	1.29×10^3	$K_{yy}^{B_4}$	2.56×10^5

Coupling (stiffness parameters)			
K_{Lxx}^C	2.12×10^5 N/m	K_{Lyy}^C	1.99×10^5 N/m
K_{Lxy}^C	1.11×10^4 N/m	K_{Lyx}^C	1.31×10^4 N/m
$K_{\varphi x \varphi x}^C$	2.20×10^5 Nm/rad	$K_{\varphi y \varphi y}^C$	2.50×10^5 Nm/rad

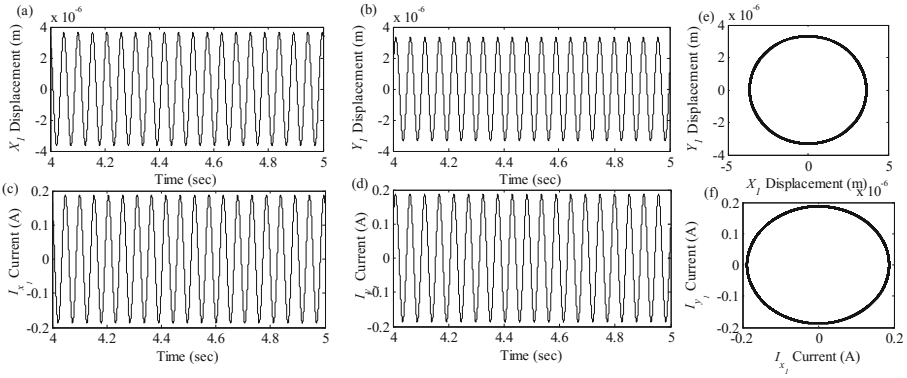

Fig. 3. A typical simulated response with respect to time for (a) horizontal displacement (b) vertical displacement (c) horizontal current (d) vertical current and orbit plot for (e) shaft centerline (f) current

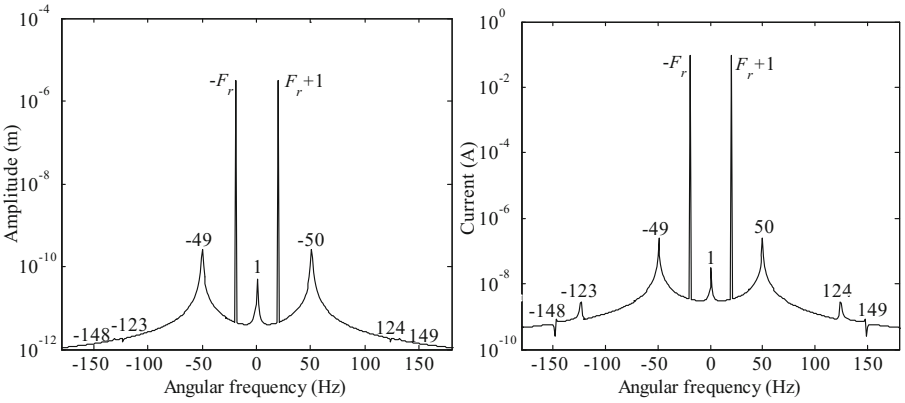

Fig. 4. Full spectrum plot (a) displacement amplitude (b) current amplitude

3 Development of Identification Algorithm Using Dynamic Condensation

By taking the solution of Eq. (8), as, $v(t) = \bar{v}(t)e^{j\omega t}$ and $i_c(t) = \bar{I}_c(t)e^{j\omega t}$, substituting these along with force as, $\bar{f}_{unb}(t) = \bar{F}_{unb}(t)$ in Eq. (8) (here $v(t), i_c(t)$ and $\bar{f}_{unb}$ are the displacement, current and residual unbalance force vector are used for converting the time domain signals EOM in to frequency domain), the EOMs in frequency domain could be expressed as,

$$\left[\left(-\omega^2\bar{M}^G_{32\times32}\right)+j\omega\left(\bar{C}^G_{32\times32}-\omega\bar{G}^G_{32\times32}\right)+\bar{K}^G_{32\times32}\right]\{\bar{v}\}_{32\times1} = \{\bar{F}_{unb}\}_{32\times1}-\{\bar{F}_{AMB}\}_{32\times1} \tag{9}$$

In practical situation, due to the limitation of number of sensors the accessibility of all the DOFs is limited and difficulty in measuring the rotational DOFs, a dynamic condensation technique has been applied. To obtain condensed EOM Eq. (9), could be divided into sub-matrices corresponding to masters and slave DOFs as,

$$\left(-\omega^2\begin{bmatrix} M^D_{mm} & M^D_{ms} \\ M^D_{sm} & M^D_{ss}\end{bmatrix}+\begin{bmatrix} K^D_{mm} & K^D_{ms} \\ K^D_{sm} & K^D_{ss}\end{bmatrix}+\mathrm{j}\omega\left(\begin{bmatrix} C^D_{mm} & C^D_{ms} \\ C^D_{sm} & C^D_{ss}\end{bmatrix}-\omega\begin{bmatrix} G^D_{mm} & G^D_{ms} \\ G^D_{sm} & G^D_{ss}\end{bmatrix}\right)\right)\begin{Bmatrix}\{v^D_m\}_{20\mathrm{x}1}\\ \{v^D_s\}_{12\mathrm{x}1}\end{Bmatrix} = \begin{Bmatrix}\{F^D_m\}_{20\mathrm{x}1}\\ \{F^D_s\}_{12\mathrm{x}1}\end{Bmatrix} \tag{10}$$

where subscripts m and s represent the master and slave DOFS respectively. Master DOFs are those DOFs that needs to retain in EOMs whereas, slave DOFs are those DOFs that could be eliminated from EOMs. Superscript 'D' stands for dynamic condensation. After splitting Eq. (10) into two equations and with mathematical rearrangement it could be written as,

$$\{v^D_s\}_{12\times1} = -\left([K^D_{ss}]_{12\times12}-\omega^2[M^D_{ss}]_{12\times12}\right)^{-1}\left([K^D_{sm}]_{12\times20}-\omega^2[M^D_{sm}]_{12\times20}\right)\{v^D_m\}_{20\times1} \tag{11}$$

With an identity matrix, state vector $\{v^D_m\}_{20\times1}$, can be written as,

$$\{v^D_m\}_{20\times1} = [I]_{20\times20}\{v^D_m\}_{20\times1} \tag{12}$$

Equations (11) and (12), can be combined as,

$$\begin{Bmatrix}\{v^D_m\}_{20\times1}\\ \{v^D_s\}_{12\times1}\end{Bmatrix} = [T^D]_{32\times20}\{v^D_m\}_{20\times1} \tag{13}$$

With

$$[T^D]_{32\times20} = \begin{bmatrix} [I]_{20\times20} \\ \hline -\left([K^D_{ss}]_{12\times12}-\omega^2[M^D_{ss}]_{12\times12}\right)^{-1}\left([K^D_{sm}]_{12\times20}-\omega^2[M^D_{sm}]_{12\times20}\right)\end{bmatrix} \tag{14}$$

where [T] is the transformation matrix for the dynamic condensation. Upon substituting Eq. (14), into Eq. (9), the resulting equation becomes as,

$$\left[\left(-\omega^2[M^D]_{20\times20}\right)+\mathrm{j}\omega\left([C^D]_{20\times20}-\omega[G^D]_{20\times20}\right)+[K^D]_{20\times20}\right]\{v^D\}_{20\times1} = \{F^D_{unb}\}_{20\times1}-\{F^D_{AMB}\}_{20\times1} \tag{15}$$

With

$$\begin{aligned}\left[M^D\right]_{20\times20} &= \left[T^D\right]^T_{20\times32}\left[\bar{M}^G\right]_{32\times32}\left[T^D\right]_{32\times20},\ \left[K^D\right]_{20\times20}\\ &= \left[T^D\right]^T_{20\times32}\left[\bar{K}^G\right]_{32\times32}\left[T^D\right]_{32\times20},\end{aligned}$$

$$\begin{aligned}\left[C^D\right]_{20\times20} &= \left[T^D\right]^T_{20\times32}\left[\bar{C}^G\right]_{32\times32}\left[T^D\right]_{32\times20},\ \left[G^D\right]_{20\times20}\\ &= \left[T^D\right]^T_{20\times32}\left[\bar{G}^G\right]_{32\times32}\left[T^D\right]_{32\times20},\end{aligned}$$

$$\left\{F^D_{unb}\right\}_{20\times1} = \left[T^D\right]^T_{20\times32}\left\{\bar{F}_{unb}\right\}_{32\times1},\ \left\{F^D_{AMB}\right\}_{20\times1} = \left[T^D\right]^T_{20\times32}\left\{\bar{F}_{AMB}\right\}_{32\times1},$$

and

$$\left\{v^D_m\right\}_{16\times1} = \left\{x_1, y_1, x_2, y_2, x_3, y_3, x_4, \varphi_{y_4}, y_4, \varphi_{x_4}, x_5, \varphi_{y_5}, y_5, \varphi_{x_5}, x_6, y_6, x_7, y_7, x_8, y_8\right\}^T \tag{16}$$

Where $(x,\ y)$ and $(\varphi_x,\ \varphi_y)$ are linear and angular displacements in two planes, respectively. To estimate the characteristic parameters Eq. (15), could be rearranged such that all the unknown parameters i.e., AMB, coupling dynamic and residual unbalance parameters are stuck on the left hand side, whereas, all the known parameters i.e., rotor mass, gyroscopic, bearing stiffness and coupling parameters on the right hand side. After rearrangement Eq. (15) could be expressed as,

$$\begin{aligned}&-\left\{F^D_{unb}\right\}_{20\times1} + \left\{F^D_{AMB}\right\}_{20\times1} + \left[K^{D(C)}\right]_{20\times20}\left\{v^D_m\right\}_{20\times1}\\ &= \left(\omega^2\left[M^D\right]_{20\times20} - \mathrm{j}\omega\left(\left[C^D\right]_{20\times20} - \omega\left[G^D\right]_{20\times20}\right) - \left[K^{D(B+R)}\right]_{20\times20}\right)\left\{v^D_m\right\}_{20\times1}\end{aligned} \tag{17}$$

The Eq. (17), could be expressed in linear regression form as

$$[A(\omega_i)]\{X\} = [B(\omega_i)] \tag{18}$$

with

$$\{X\} = \left\{e_{1r}\ e_{1i}\ e_{2r}\ e_{2i}\ K_{sx1}\ K_{ix1}\ K_{sx2}\ K_{ix2}\ K_{sy1}\ K_{iy1}\ K_{sy2}\ K_{iy2}\ K^C_{Lxx}\ K^C_{Lxy}\ K^C_{Lyx}\ K^C_{Lyy}\ K^C_{\varphi_x\varphi_x}\ K^C_{\varphi_y\varphi_y}\right\}$$

The associated regression matrices $[A]$ and $[B]$ in complex form are presented in Appendix. Regression matrix $[A]$ contains contributions due to unknown parameter i.e., residual unbalances (F^D_{unb}), AMB force (F^D_{AMB}) (force–displacement and force current stiffness) and coupling stiffness $(K^{D(C)})$. The matrix $[B]$ contains the contributions due to known parameter i.e., mass (M^D) (shaft and disc), stiffness $(K^{D(B+R)})$ (bearing and coupling), damping (C^D) (rotor) and gyroscopic effect (G^D). The Eq. (18), requires an independent set of displacement and current response information to estimate the characteristic parameters kept in vector $\{X\}$. Here vector $\{X\}$ contains e_{1r}, e_{1i}, e_{2r} and e_{2i} are the residual unbalances real and imaginary values, $K_{sx_1}, K_{ix_1}, K_{sx_2}, K_{ix_2}, K_{sy_1}, K_{iy_1}, K_{sy_2}$ and K_{iy_2} are the force displacement and force

current along x and y directions and $K^C_{Lxx}, K^C_{Lxy}, K^C_{Lyx}, K^C_{Lyy}, K^C_{\varphi_x\varphi_x}$ and $K^C_{\varphi_y\varphi_y}$ are the coupling linear, cross and angular parameters.

4 Parameter Estimation

In this section, procedure to obtain independent sets of measurement response and parameters estimation is presented. To have the effects of different modes of excitation in the identification algorithm, displacement and current responses are generated at selected operating speeds, in between 2nd and 3rd natural frequency i.e., 16 Hz, 17 Hz, 18 Hz, 19 Hz, 20 Hz, 21 Hz, 22 Hz, 23 Hz, 24 Hz, and 25 Hz. The estimated characteristic parameters and percentage deviation for various levels of measurement noise are presented in Table 2 and percentage deviation plot is shown in Fig. 5. From Table 2 and Fig. 5, it can be seen that most of the estimated parameters exhibit good agreement with assumed values up to 10% measurement noise. It could be concluded that the unbalance parameter i.e. eccentricity exhibits maximum deviation 9.61% for 10% measurement noise condition. With the careful investigation of absolute value of eccentricity it could be concluded that although, relative deviation is highest for eccentricity but absolute deviation is very less.

Table 2. Percentage deviation in estimated parameters with addition of measurement noise

Parameters	Assumed values	Estimated parameters		
		0% Noise	5% Noise	10% Noise
		Est. values (% Error)	Est. values (% Error)	Est. values (% Error)
e_1	2.40×10^{-4}	2.39×10^{-4} (0.34)	2.51×10^{-4} (4.63)	2.61×10^{-4} (9.61)
e_2	2.40×10^{-4}	2.36×10^{-4} (1.66)	2.50×10^{-4} (4.16)	2.60×10^{-4} (8.33)
K_{sx1}	1.05×10^5	1.05×10^5 (0.01)	1.05×10^5 (0.01)	1.05×10^5 (0.01)
K_{ix1}	42.00	41.95 (0.10)	41.95 (0.10)	41.95 (0.10)
K_{sx2}	1.05×10^5	1.05×10^5 (0.04)	1.05×10^5 (0.04)	1.05×10^5 (0.04)
K_{ix2}	42.00	41.95 (0.10)	41.95 (0.10)	41.95 (0.10)
K_{sy1}	1.05×10^5	1.05×10^5 (0.01)	1.05×10^5 (0.01)	1.05×10^5 (0.01)
K_{iy1}	42.00	41.95 (0.10)	41.95 (0.10)	41.95 (0.10)
K_{sy2}	1.05×10^5	1.05×10^5	1.05×10^5	1.05×10^5

(*continued*)

Table 2. (*continued*)

Parameters	Assumed values	Estimated parameters		
		0% Noise	5% Noise	10% Noise
		Est. values (% Error)	Est. values (% Error)	Est. values (% Error)
		(0.03)	(0.03)	(0.03)
K_{iy2}	42.0	41.95 (0.11)	41.95 (0.11)	41.95 (0.11)
K^c_{Lxx}	2.12×10^5	2.11×10^5 (0.00)	2.11×10^5 (0.00)	2.11×10^5 (0.00)
K^c_{Lxy}	1.11×10^5	1.10×10^5 (0.00)	1.10×10^5 (0.00)	1.10×10^5 (0.00)
K^c_{Lyx}	1.31×10^5	1.31×10^5 (0.22)	1.31×10^5 (0.22)	1.31×10^5 (0.22)
K^c_{Lyy}	1.99×10^5	1.99×10^5 (0.04)	1.99×10^5 (0.04)	1.99×10^5 (0.04)
$K^c_{\varphi x \varphi x}$	2.20×10^5	2.20×10^5 (0.00)	2.20×10^5 (0.00)	2.20×10^5 (0.00)
$K^c_{\varphi y \varphi y}$	2.50×10^5	2.50×10^5 (0.00)	2.50×10^5 (0.00)	2.50×10^5 (0.00)

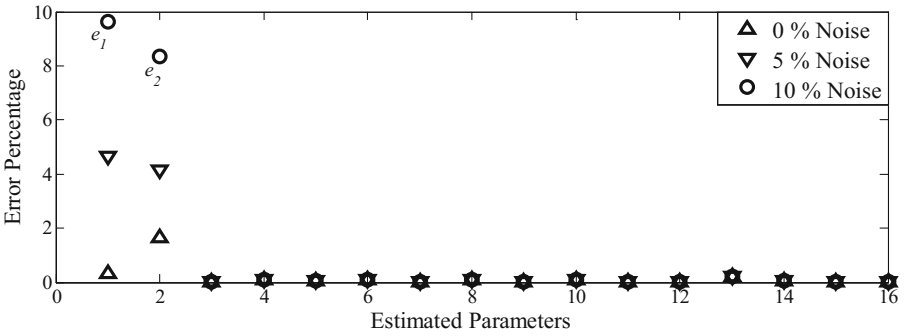

Fig. 5. Error plot of estimated parameters for different level of measurement noise

5 Conclusions

In this article, an identification algorithm based on least squares technique is developed to estimate the characteristic parameters of inherent unbalance, AMB and coupling misalignment dynamic parameters for the AMB integrated rotor–bearing–coupling system. Euler Bernoulli beam theory is applied to model flexible shafts and finite element method is applied to develop equations of motion. Although, finite element method is more accurate and realistic approach to model real rotor test rigs but the

degrees of freedom of the system increases as the number of node increases. Accessibility of all these degrees of freedom and accurate measurements of angular degrees of freedom are the most challenging problems in the real rotor test rigs. To overcome this difficulty, a dynamic reduction technique is applied in the developed identification algorithm to eliminate some linear and all angular degrees of freedom. The identification algorithm developed requires current and displacement responses in frequency domain along with system's model information. The fault parameters estimated are coupling misalignment, inherent unbalance along with AMBs characteristic parameters. The effectiveness and robustness of the proposed methodology is tested against measurement error by incorporating different levels of measurement noise.

Appendix

The regression matrices are developed according to the frequency peaks ($fr + 1$, 149, 124, 50, 0, −49, −123, $-148 - fr$) obtained in the FFT plot (refer Fig. 4).

$$[A(\omega_i)]_{360\times 18}\{X\}_{18\times 1} = [B(\omega_i)]_{360\times 1}$$

with

$$[A(\omega_i)]_{360\times 18} = \left[\left[A^{unb}(\omega_i)\right]\left[A^{AMB}(\omega_i)\right]\left[A^{C}(\omega_i)\right]\right]_{360\times 18}$$

where $[A^{unb}]$ is the contribution due to residual unbalances, $[A^{AMB}]$ is the contribution due to AMB stiffness and $[A^{C}]$ is the contribution due to coupling stiffness. Details of $[A^{unb}]$, $[A^{AMB}]$ and $[A^{C}]$ are shown below,

Elements of regression matrix $[A^{unb}]$

$$A^{unb}(1,1) = A^{unb}(182,2) = -m^{d_1}\omega^2\lambda_{unb1};\ A^{unb}(1,3) = A^{unb}(184,4) = -m^{d_2}\omega^2\lambda_{unb2};$$

Elements of regression matrix $[A^{AMB}]$

$$\left[A^{AMB}(\omega_i)\right] = \begin{bmatrix} re\left(\bar{\eta}_i^{\circ}\lambda_{xAMB_1}\right) & re\left(I_i\lambda_{xAMB_1}\right) & re\left(\bar{\eta}_i^{\circ}\lambda_{xAMB_2}\right) & re\left(I_i\lambda_{xAMB_2}\right) \\ \vdots & \vdots & \vdots & \vdots \\ im\left(\bar{\eta}_i^{\circ}\lambda_{yAMB_1}\right) & im\left(I_i\lambda_{yAMB_1}\right) & im\left(\bar{\eta}_i^{\circ}\lambda_{yAMB_2}\right) & im\left(I_i\lambda_{yAMB_2}\right) \\ \vdots & \vdots & \vdots & \vdots \end{bmatrix}$$

Elements of regression matrix $[A^{C}]$

$$[A^C(\omega_i)] = \begin{bmatrix} re(\bar{\eta}_i\lambda^c_{Lxx}) & re\left(\bar{\eta}_i\lambda^c_{Lxy}\right) & re\left(\bar{\eta}_i\lambda^c_{Lyx}\right) & re\left(\bar{\eta}_i\lambda^c_{Lyy}\right) & re\left(\bar{\eta}_i\lambda^c_{\varphi_x\varphi_x}\right) & re\left(\bar{\eta}_i\lambda^c_{\varphi_y\varphi_y}\right) \\ \vdots & \vdots & \vdots & \vdots & \vdots & \vdots \\ im(\bar{\eta}_i\lambda^c_{Lxx}) & im\left(\bar{\eta}_i\lambda^c_{Lxy}\right) & im\left(\bar{\eta}_i\lambda^c_{Lyx}\right) & im\left(\bar{\eta}_i\lambda^c_{Lyy}\right) & im\left(\bar{\eta}_i\lambda^c_{\varphi_x\varphi_x}\right) & im\left(\bar{\eta}_i\lambda^c_{\varphi_y\varphi_y}\right) \\ \vdots & \vdots & \vdots & \vdots & \vdots & \vdots \end{bmatrix}$$

Elements of regression matrix $[B]$

$$[B(\omega_i)] = \begin{bmatrix} \omega^2 M^D re(\bar{\eta}_i) - K^{D(R+B)} re(\bar{\eta}_i) + \omega C^D im(\bar{\eta}_i) + \omega^2 G^D im(\bar{\eta}_i) \\ \vdots \\ \omega^2 M^D im(\bar{\eta}_i) - K^{D(R+B)} im(\bar{\eta}_i) + \omega C^D re(\bar{\eta}_i) + \omega^2 G^D re(\bar{\eta}_i) \\ \vdots \end{bmatrix}$$

Here $\bar{\eta}_i$ and I_i ($i = fr + 1, 149, 124, 50, 0, -49, -123, -148 - fr$) are the frequency and current responses. λ_{unb_i} ($i = 1$ & 2), λ_{xAMB_i}, λ_{yAMB_i}, ${}^o\lambda_{xAMB_i}$, ${}^o\lambda_{yAMB_i}$($i = 1$ and 2)λ^C_{Lxx}, λ^C_{Lxy}, λ^C_{Lyx}, λ^C_{Lyy}, $\lambda^C_{\varphi_x\varphi_x}$, $\lambda^C_{\varphi_y\varphi_y}$ are the flag position and responses of the unbalance, AMB (displacement and current along x and y directions) and coupling (linear, cross–coupling and angular).

References

1. Leung AYT (1978) An accurate method of dynamic condensation in structural analysis. Int J Numer Meth Eng 12(11):1705–1715
2. Paz M (1989) Modified dynamic condensation method. J Struct Eng 115(1):234–238
3. Ahn HJ, Lee SW, Lee SH, Han DC (2003) Frequency domain control-relevant identify cation of MIMO AMB rigid rotor. Automatica 39(2):299–307
4. Lees AW, Friswell MI (2006) Where next for condition monitoring of rotating machinery. Adv Vibr Eng 5(4):263–277
5. Das AS, Nighil MC, Dutt JK, Irretier H (2008) Vibration control and stability analysis of rotor-shaft system with electromagnetic exciters. Mech Mach Theory 43(10):1295–1316
6. Rao JS (2011) History of rotating machinery dynamics. Springer, Dordrecht (2011)
7. Lal M, Tiwari R (2012) Multi–fault identification in simple rotor–bearing–coupling systems based on forced response measurements. Mech Mach Theory 51:87–109
8. Lal M, Tiwari R (2012) Identification of multiple faults with incomplete response measurements in rotor-bearing-coupling systems. In: ASME gas turbine India conference, pp 613–620
9. Lal M, Tiwari R (2013) Quantification of multiple fault parameters in flexible turbo-generator systems with incomplete rundown vibration data. Mech Syst Signal Process 41(1–2):546–563
10. Lal M, Tiwari R (2013) Identification of multiple faults in rigid rotor and flexible bearing-coupling system—an experimental investigation. In: ASME gas turbine India conference, p V001T05A020
11. Sun Z, He Y, Zhao J, Shi Z, Zhao L, Yu S (2014) Identification of active magnetic bearing system with a flexible rotor. Mech Syst Signal Process 49(1):302–316

12. Lal M, Tiwari R (2015) Experimental estimation of misalignment effects in rotor-bearing-coupling systems. In: Proceedings of the 9th IFToMM international conference on rotor dynamics, mechanisms and machine science, vol 21, pp 779–789
13. Singh S, Tiwari R (2016) Model-based switching-crack identification in a Jeffcott rotor with an offset disk integrated with an active magnetic bearing. J Dyn Syst Meas Contr 138 (3):031006
14. Zhou J, Di L, Cheng C, Xu Y, Lin Z (2016) A rotor unbalance response based approach to the identification of the closed-loop stiffness and damping coefficients of active magnetic bearings. Mech Syst Signal Process 66:665–678
15. Xu Y, Zhou J, Lin Z, Jin C (2018) Identification of dynamic parameters of active magnetic bearings in a flexible rotor system considering residual unbalances. Mechatronics 49:46–55